International Journal of Applied Earth Observations and Geoinformation 108 (2022) 102740

Contents lists available at ScienceDirect

International Journal of Applied Earth Observations and Geoinformation

journal homepage: www.elsevier.com/locate/jag

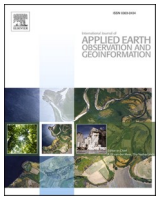

Early detection of tree encroachment in high voltage powerline corridor using growth model and UAV-borne LiDAR

Yangyu Chen [a,b], Jiayuan Lin [a,b,*], Xiaohan Liao [c]

[a] Chongqing Jinfo Mountain Karst Ecosystem National Observation and Research Station, School of Geographical Sciences, Southwest University, Chongqing 400715, China
[b] Chongqing Engineering Research Center for Remote Sensing Big Data Application, School of Geographical Sciences, Southwest University, Chongqing 400715, China
[c] Institute of Geographic Sciences and Natural Resources Research, Chinese Academy of Sciences, Beijing 100101, China

ARTICLE INFO

Keywords:
Powerline corridor
Tree encroachment
Point cloud
Richards growth model
Bounding box
Intersection test

ABSTRACT

UAV-borne LiDAR is an innovative and effective technique for tree encroachment detection in high voltage powerline corridor. However, the periodical inspection of the whole powerline corridor is inefficient, as the powerline segments occurring the tree encroachment only account for a very small part. In this paper, taking one segment of the powerline corridor in Taining County, Fujian province, China as the test site, we acquired the point cloud data using a UAV-borne LiDAR, and then combined the tree growth model and two-phase encroachment detection algorithm to realize efficiently early detection of tree encroachment. First, the points of powerlines and trees were classified from the point cloud, and then the individual tree heights and the belonging tree species were extracted. Based on tree plot data, the relationships between tree heights and tree ages were established using Richards growth model. Secondly, the individual tree heights were predicted at given time points, and the tree encroachments were detected in advance according to the required safe distance between powerlines and trees. To tackle the huge amount of point cloud data and calculation, the two-phase tree encroachment detection algorithm based on bounding boxes was applied to replace the traditional point traversal algorithm. As a result, the exact locations of tree encroachment were early detected and the specific encroaching trees were also pre-identified. Lastly, the pre-detected tree encroachment should be verified through field survey, and treated accordingly. Thus, the inspection efficiency would be greatly improved. In accuracy assessment, the coefficient of determination (R^2) and the root mean square error (RMSE) of fitted growth model for Masson pine were 0.812 and 2.308 m, and 0.861 and 2.556 m for Eucalyptus, respectively. Compared with point traversal algorithm, the calculation efficiency of the two-phase tree encroachment detection algorithm was improved by nearly 76 times on average.

1. Introduction

High voltage powerlines are the important infrastructure to transmit electric power for daily life and industrial production (Guo et al., 2016; Ortega et al., 2019). The neighboring three-dimensional (3D) space surrounding the powerlines and the relevant facilities is usually called the powerline corridor. In the corridor, the other things such as buildings and plants should keep a certain safe distance from the powerlines. Generally, the safe distance becomes longer accordingly with the increase of the voltage. Due to the long transmission distance and large coverage area of the power grid, some powerlines have to pass across large forests in mountainous areas. The neighboring trees often grow into the safe space of the powerlines, probably causing power outages or start a fire in the surrounding forest (Ahmad et al., 2013; Liu et al., 2019; Ma et al., 2020). Therefore, it is of significant value to timely detect and fell trees encroaching into the safe space of high voltage powerlines.

The traditional powerline inspection is done via field survey. The inspectors observe and roughly estimate the distance between the powerlines and the underneath forest (Mills et al., 2010; Wang et al., 2017). This method has a long inspection cycle and intensive workload. Some powerline segments cannot be regularly inspected due to the steep terrain and dense forest. With the advantages of low cost, flexible take-off and landing, safety, flying under clouds, and hyperspatial image resolution (Lin et al., 2012), unmanned aerial vehicle (UAV) remote

* Corresponding author at: Chongqing Jinfo Mountain Karst Ecosystem National Observation and Research Station, School of Geographical Sciences, Southwest University, Chongqing 400715, China.
E-mail address: joeylin@swu.edu.cn (J. Lin).

https://doi.org/10.1016/j.jag.2022.102740
Received 9 December 2021; Received in revised form 23 February 2022; Accepted 6 March 2022
Available online 11 March 2022

sensing has been increasingly used for powerline inspection. The optical images or videos of the powerline corridor are first caught using UAV-borne digital camera, and then the technical staff can directly observe and judge whether or not the neighboring trees have grown into the powerline safe space (Matikainen et al.,2016; Nguyen et al., 2018). Although the inspection efficiency and spatial accessibility are improved, the inspecting results are still affected by human factors. Actually, the 3D scene of powerline corridor can be reconstructed based on the overlapping UAV-acquired images using Structure from Motion (SfM) photogrammetry (Huang et al.,2021). Thus, the distances between the powerlines and the surrounding trees can be accurately measured, and the tree encroachment can be quantitatively detected. However, the powerline is often unable to be correctly matched between overlapping images due to its thin diameter, image quality, and scene complexity.

In recent years, UAV-borne LiDAR has become the most popular tool for tree encroachment detection. The accurate 3D scene along the powerline corridor can be obtained using the laser ranging data and the instantaneous position of the LiDAR itself (Azevedo et al., 2019). Based on the resulting 3D point cloud, the powerlines can be correctly extracted (Cheng et al., 2014; Guan et al., 2016; Hartling et al., 2021), and the distances between the powerlines and the underneath forest can be precisely measured (Chen et al., 2018; Shi et al., 2020; Dihkan et al., 2021). When the distance is less than the required safe value, the tree encroachment is believed to have occurred. Usually, the distances between each pair of powerline point and tree point are calculated in an ergodic way (Ding et al., 2018; Ruan et al., 2019), requiring a large amount of calculation. Fu et al. (2019) established the virtual grid of ground objects and calculated the distances between powerlines and grid cells to improve efficiency. Zhang et al. (2020a) segmented the powerlines and calculated the distances between powerline segments and underneath forest. Although the detection speed was accelerated, there existed the problem of missing detection. Therefore, the huge amount of data and calculation is always a big challenge in tree encroachment detection using laser scanned point cloud.

In fact, the continuous growth of trees is the major reason why the powerline corridor needs periodical inspection. As the trees grow higher, the distances between the powerline and trees are reduced. As a result, the previous powerline inspection was out of date. Therefore, the powerlines have to be periodically inspected for new tree encroachments. As the powerline segments occurring tree encroachment only account for a very small part, periodical inspections of the whole powerline corridor are so inefficient and most inspections are in vain. According to the studies (Fox et al., 2001; Collet et al., 2006), tree growth also follows certain laws and can be modeled using some measurable factors including tree height, diameter at breast height (DBH), soil organic matter, sunlight, etc.. Tree growth models can be divided into two categories, namely empirical models and theoretical models. The empirical models are actually based on statistics, and require huge sample data (Calama et al.,2008). As for the theoretical models such as Richards model, their parameters generally have certain biological meanings (Shoda et al., 2020). Comparatively, they can better explain tree growth process and predict tree growth trend. Therefore, it seems a very promising method to predict tree height growth and detect potential tree encroachments in advance. Huang et al. (2017) carried out early-warning analysis of tree barriers in the powerline corridor using Richards model, providing a reference framework for implementation. To deal with the oscillation of powerlines caused by the wind, Wu et al. (2021) combined a wire sag model with tree growth model to predict tree barriers more accurately. Thus powerline inspectors can be sent out to properly treat the predicted tree barriers (namely tree encroachments), and the inspection efficiency will be greatly improved. However, the two studies have not incorporated the UAV-borne LiDAR and tackled the sharply increased amount of point data calculation caused by time series pre-detection of tree encroachments.

In this paper, we aim to combine Richards growth model and UAV-borne LiDAR to realize early detection of tree encroachment in high voltage powerline corridor. The major contributions include: (1) systematically demonstrating the procedures of incorporating point cloud data into pre-detecting tree encroachments in the powerline corridor; (2) proving the optimum adaptability of Richards model in tree growth modeling, and establishing growth models of two tree species (Masson pine and Eucalyptus) to predict underneath tree heights more exactly; (3) applying bounding box-based two-phase algorithm to tackling the dramatically increased amount of point data calculation posed by long time series pre-detection of tree encroachments.

2. Study area and data

2.1. Study area

As shown in Fig. 1a, the study area is located in Taining County, Fujian Province, China. This area has a typical subtropical monsoon climate with a mean annual temperature of 17 °C and a mean annual rainfall of 1,725 mm. The principle vegetation type is the evergreen broad-leaved forest which are usually distributed in the mid-subtropical zone. The dominant tree species in this region include Eucalyptus (Eucalyptus robusta Smith), Masson pine (Pinus massoniana Lamb), China fir (Cunninghamia lanceolata), etc. Passing across the mid-east of Taining County, the Chixin high voltage (220kv) powerlines has a length of 28 km, and the required safe clearance distance between the powerlines and ground objects is 6 m. As indicated in Fig. 1b, one segment of Chixin powerlines and the neighborhood was chosen as the test site. The two towers at both ends, the powerlines, and the underneath forest can be observed in the orthoimage. The distance between the two towers is about 500 m. According to the field investigation, there are only two tree species in the underneath forest, namely Masson pine and Eucalyptus. Therefore, it is an ideal test site for studying on combining UAV-borne LiDAR and tree growth model to early detect tree encroachment.

2.2. Data

2.2.1. LiDAR point cloud

The Tovos DroneScan loaded on the DJI Matrice 600 Pro was utilized to collect point cloud data of the test site. The drone is a 6-rotor aircraft with a load of up to 6 kg. The LiDAR has a scanning frequency of 300,000 points per second, a scanning accuracy of 5 cm, and a weight of about 2.5 kg. During the UAV flight, the heading and side overlap rates were set to 80% and 90%, respectively. The flight speed was set to 1 m/s, and the relative flight altitude was 40 m. The data scanned and collected by the laser scanner was first recorded in raw format, and then resolved with the built-in software to obtain point cloud data in LAS format (ASPRS, 2005). As shown in Fig. 2, the acquired point cloud data includes powerlines, the two towers at both ends, and the underneath forest. The coordinate and projection system of the point cloud data and the above orthoimage is WGS 84/UTM 50 N. The elevations of the point cloud data range from 440 m to 540 m.

2.2.2. Statistical data of tree plots

According to similar site conditions, the local forestry authorities provided the statistical data of 217 plots of Masson pine and 166 plots of Eucalyptus tree respectively. As shown in Table 1, the age range of Masson pine plots is from 2 yr to 58 yr, and the corresponding tree height range is from 1.70 m to 24.55 m. The age range of Eucalyptus tree plots is from 3 yr to 50 yr, and the corresponding tree height range is from 3.0 m to 29.7 m. Among them, 80% will be used for growth model fitting and the rest 20% will be for model evaluation.

3. Methods

The procedures of early detecting tree encroachment in the powerline corridor are as follows. First, the point cloud data needs to be preprocessed to separately obtain the points of powerline and trees. The 3D

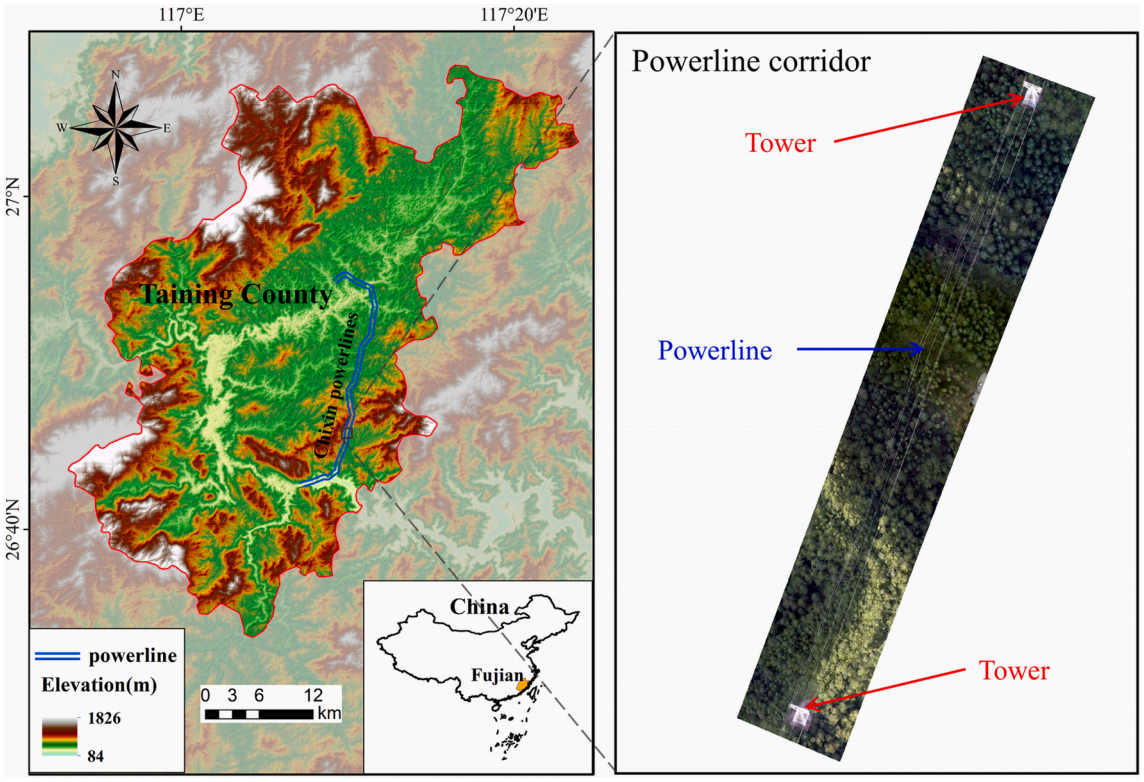

Fig. 1. (a) The location of the study area, and (b) the orthoimage of the sample segment of powerline corridor.

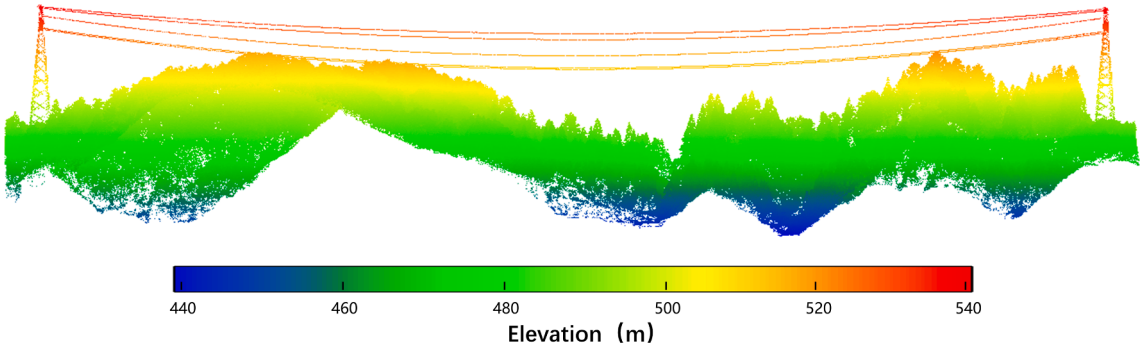

Fig. 2. The scanned point cloud of the sample segment of powerline corridor.

Table 1
The statistical data of tree plots of Masson pine and Eucalyptus.

Tree species	Plot number	Age (yr)			Height (m)		
		Max.	Min.	Avg.	Max.	Min.	Avg.
Masson pine	217	58	2	26.55	24.55	1.7	15.7
Eucalyptus	166	50	3	18.86	29.7	3	19.21

buffer of the powerline will be produced with the safe clearance distance, and segmented to generate the bounding boxes. The tree points will be segmented to extract individual trees and their heights. Secondly, the parameters of Richards growth model will be estimated based on the statistical data of tree plots. For a given time point in future, the individual tree heights at that time will be acquired by combining the current individual tree heights and the growth model. Then, the bounding boxes of individual trees at the given time point will be produced. Thirdly, the intersection test will be conducted between the bounding boxes of powerline buffer segments and individual trees. If the result is false, no tree encroachment occurs. Otherwise, the point distances between the two bounding boxes will be ergodically calculated and compared with the safe distance. If the distances are all bigger than the safe distance, there is no tree encroachment occurring. Otherwise, the tree encroachment does occur and the encroaching individual trees can be further identified. In real scenarios, multiple tree species and their growth models have to be dealt with. The overall flowchart is shown in Fig. 3.

3.1. Point cloud preprocessing

The raw point cloud data not only includes the powerlines and the vegetation, but also the irrelevant data such as non-ground points and surrounding objects. Before tree encroachment detection, the point cloud data needs to be preprocessed through denoising, filtering, and classification.

3.1.1. Point cloud denoising

While point cloud data are being scanned with UAV-borne LiDAR,

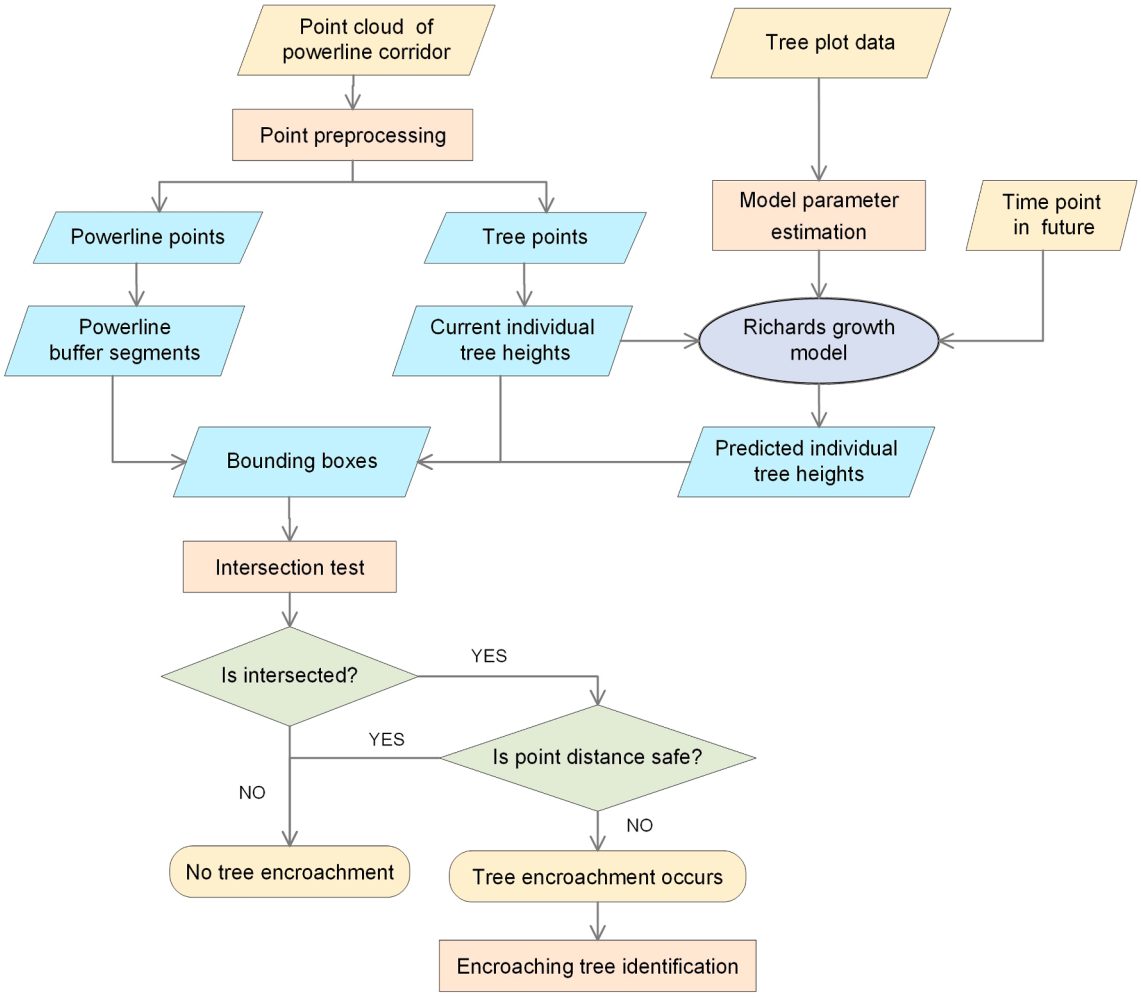

Fig. 3. The flowchart for early detecting tree encroachment in the powerline corridor.

some point outliers will be produced by the internal instability of the device or the external factors such as flying birds and terrain fluctuation. These point outliers away from the whole point cloud data are often called noise points. For subsequent point cloud classification and bounding box generation, it is necessary to eliminate the point outliers. The statistical filtering (Li et al., 2016) is used to denoise the raw point cloud. This method makes a statistical analysis of the specified neighborhood of each point and calculates its average distance to all adjacent points. The statistical result is assumed to satisfy the Gaussian distribution, thus an interval can be defined with the global mean and standard deviation of the average distances. Each point with an average distance outside of the interval will be determined as an outlier and removed.

3.1.2. Point cloud classification

a) Point filtering. Point filtering is to separate ground points from non-ground points in point cloud data. The cloth filtering method by Zhang et al. (2016) is used to filter point cloud. The method assumes that the original terrain is flipped upside down and there is a virtual cloth of enough hardness above. The cloth will eventually fall and cover the flipped terrain surface due to the force of gravity. The final shape of the cloth is actually the Digital Elevation Model (DEM). The points on the DEM are determined as ground points, and the others are non-ground ones.
b) Extraction of powerline points. Since the elevations of the powerline points are remarkably greater than those of other non-ground points, an elevation threshold can be set to only keep the powerline points and part of tower points. Then, the discrepancy of elevation change filtering method (DECF) is adopted to further separate powerline points from tower points. As the powerline between towers is usually a gentle curve, the elevation difference between powerline points is relatively small. Contrastively, the elevations of tower points have a significant variation in the vertical direction.
c) Extraction of tree points. After powerline points have been extracted, the left non-ground points mainly include vegetation points and the lower half of tower points. Therefore, tree points can be acquired just by eliminating the tower points. The center coordinates of the tower are first obtained from the point cloud, and then a cylinder that can enclose the tower is generated. As there is usually no tree under the tower, the tree points can be obtained by removing all the points in the cylinder from the left non-ground points.

3.2. Tree height prediction with growth model

3.2.1. Tree growth model

In the study, the growth models of the two tree species in the test site were established using the Richards model. It is a theoretical growth model obtained via mathematical deduction, and principally studies the relationship between tree age and tree height. Richards model is suitable for the simulation of both linear and nonlinear processes with relatively small growth rate (Wei et al., 2012). As tree growth is exactly a nonlinear process with this characteristic, Richards model is expected to make a good performance in this regard. The mathematical equation of

Richards model is as follows:

$$y = a\left(1 - e^{-bt}\right)^c \quad (1)$$

Where t represents the tree age and y represents the tree height at t age; a, b, and c are model parameters. a is the maximum tree height, b is related to the tree growth rate, and c reflects the position of the inflection point in the growth curve.

All of the model parameters in Eq. (1) have their own biological significance. The parameter b is determined by tree age, site conditions, average DBH and tree density. Among them the tree age has the greatest determination on the value of b. The exact position of inflection point influences the shape of the growth curve, therefore the parameter c is closely related to the accuracy of growth simulation. With different parameter values and their combinations, the models represent different biological growth.

The specific values of model parameters will be estimated using the nonlinear least square method(LSM) (Wei et al.,2012), which is actually a mathematical optimization process. It obtains the best function matching of sample data by minimizing the sum of squares of errors. For nonlinear Richards model, we can use the Marquardt method (Fan,2012) to transform the nonlinear LSM problem into a series of linear LSM problem, which can subsequently be solved via iteration. The procedures of estimating the parameters in Eq. (1) are as follows:

a) The initial parameter values of Richards growth model for one tree species are estimated according to the empirical values and the average tree heights at various ages.
b) The Marquardt method is used to optimize the model parameters, and the tentative parameter values will be obtained.
c) The fitting degree of the model with the tentative parameters is evaluated. If it does not meet the requirement, the procedure will go to previous step.

According to the above steps, the Richards growth models of Masson pine and Eucalyptus are established with the estimated parameter values respectively.

3.2.2. Tree height prediction

In order to predict individual tree heights at the future time point using Richards growth model, the current ages and belonging species of individual trees should be determined. First, it is necessary to segment individual trees from the vegetation point cloud obtained in Section 3.1.2. The normalized cut method proposed by Li et al.(2012) is used for this purpose. The local maximum points of the point cloud are extracted as the initial tree tops, which will be used as the seed points for subsequent iterative processing. The average half horizontal distance between the neighboring tree tops will be taken as the distance threshold. The circular region centered on the seed point expands outward, and the points falling in the projected cylinder are judged according to the distance threshold. If the distance of a point is less than the threshold value, the point is determined to belong to the current individual tree. If the point distance is greater than the threshold value, the point surely belongs to another individual tree. After segmenting individual trees from point cloud, their spatial positions and tree heights can be conveniently extracted. The belonging species (Masson pine or Eucalyptus) of individual trees is determined by visual interpretation of the corresponding orthoimage and field investigation.

Next, the current individual tree ages can be reversely calculated by inputting the individual tree heights into Richards growth models. The time span from the current to the given time point should be converted into a time length in year unit. The individual tree ages at the given time point can be obtained by adding the time span to the current individual tree ages. Lastly, the individual tree heights at the given time point can be achieved using Richards growth models of the corresponding tree species.

3.3. Two-phase tree encroachment detection

Tree encroachment detection in the powerline corridor is done by comparing the specified safe distance with the real distances between individual trees and powerlines. Traditionally, it needs to traverse and calculate the distance between each pair of powerline point and tree point. As the LiDAR points of powerlines and underneath trees are usually huge, the traditional method requires a large amount of calculations and takes a long time. To improve the calculation efficiency, the two-phase tree encroachment algorithm based on bounding boxes is applied. The tree encroachment detection in the powerline corridor will be transformed into the intersection tests between the bounding boxes enclosing powerlines and underneath individual trees.

The bounding box is a commonly used tool in collision detection among 3D geometric objects. The basic idea is to enclose complex geometric objects with slightly larger and simple 3D geometric shapes such as cuboid, sphere, and cone (Palmer and Grimsdale, 1995; Gottschalk et al., 1996). Before the collision detection of two complex geometric objects, the intersection test between the two bounding boxes enclosing them will be first carried out. If the bounding boxes are not intersected, the two geometric objects do not collide with each other for sure. Otherwise, the direct collision tests between the two geometric objects will be further performed. The intersection test between bounding boxes is much simpler and faster than the direct collision detection between complex geometric objects. As most geometric objects do not collide in real scenario, the bounding box-based intersection test can exclude overwhelming majority of nonintersecting objects. In this way, the total efficiency of collision detection is greatly improved.

3.3.1. Bounding box generation

The bounding boxes enclosing point cloud are mainly categorized into Axis-Aligned Bounding Box (AABB) and Oriented Bounding Box (OBB), etc. (Tang et al.,2018). As relatively easier to generate, the AABB is adopted in this study. The AABB is defined as the smallest hexahedron that encloses a point cloud object and each side of it is parallel to one of the X, Y and Z coordinate axes. The AABB of a given object is obtained by traversing all the points belonging to the object to find the maximum and minimum values of X, Y and Z coordinates of those points. The 6 coordinate extreme values constitute the 8 vertices of the bounding box (Xing et al., 2010).

Before detecting tree encroachment, the AABB bounding boxes should be generated for powerline points and vegetation points respectively. For the multilayer powerlines in vertical direction, only the powerline in the lowest lay is taken into consideration. The Euclidean clustering is first performed on the classified powerline points to separate individual powerlines. The lowest powerline will be selected to generate a 3D buffer with a width of the required safe distance. The resulting buffer will be used as the enclosed geometric object to generate the bounding box of the corresponding powerline. To further improve the detection efficiency, the powerline buffer is segmented along the X axis. As shown in Fig. 4, it is actually the bounding boxes for the powerline buffer segments that will be used for tree encroachment detection. However, the detection efficiency is not always improved with the increasing of the segment number. The appropriate number of segments needs to be determined through experiments. Comparatively, it is much simpler to generate the bounding boxes for individual trees (see Fig. 4), whose points have been separately extracted in Section 3.2.2.

3.3.2. Bounding box intersection test

The intersection test between two AABB bounding boxes is equivalent to judging whether their projection intervals are simultaneously overlapped in the three coordinate axes. Every 4 sides of the AABB bounding box are parallel to the X, Y and Z coordinate axes respectively. The coordinates of the two end vortexes of the 4 sides determine the projection interval of the bounding box in the corresponding coordinate axis. Generally, the intersection test between two AABB bounding boxes

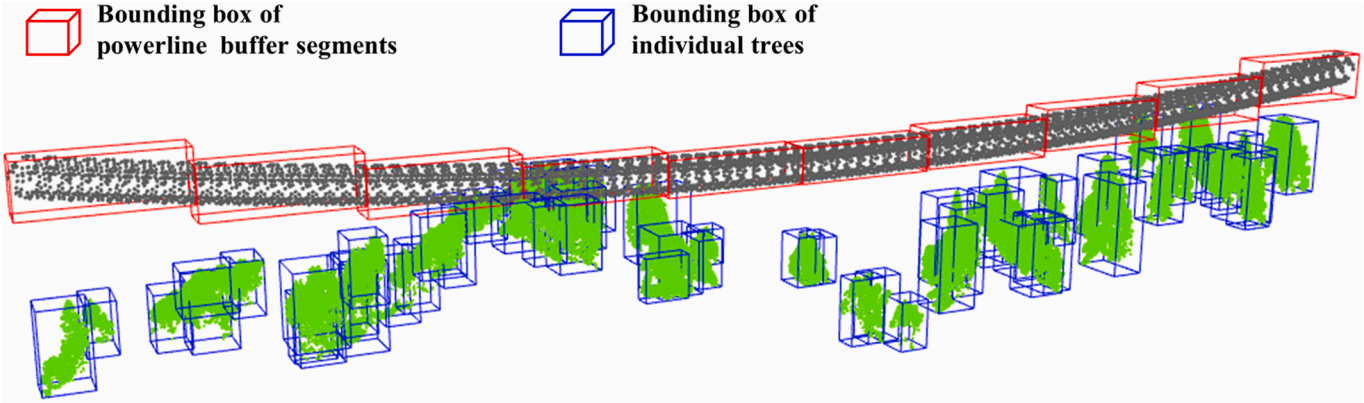

Fig. 4. The bounding boxes of powerline buffer segments and underneath individual trees.

only needs 6 comparison operations at most (Yu et al., 2018).

As shown in Fig. 5, the bounding box of one powerline buffer segment is denoted as P, and that of an individual tree is T. In most cases, P and T are not intersected (Fig. 5a). The P and T is intersected only if the Eqs. (2)–(4) are simultaneously satisfied.

$$((T_{xmin} > P_{xmax} || (T_{xmax} < P_{xmin})) == 0 \tag{2}$$

$$((T_{ymin} > P_{ymax} || (T_{ymax} < P_{ymin})) == 0 \tag{3}$$

$$((T_{zmin} > P_{zmax} || (T_{zmax} < P_{zmin})) == 0 \tag{4}$$

Where the subscripts *xmin*, *xmax*, *ymin*, *ymax*, *zmin*, and *zmax* represent the boundary values of the projection intervals of the two bounding boxes in the three coordinate axes respectively.

In the case of tree encroachment detection, Eq. (4) can be further simplified as Eq. (5), because the trees can only encroach on the powerline corridor from down to up direction.

$$(T_{zmax} \geq P_{zmin}) == 1 \tag{5}$$

3.3.3. Encroaching tree identification and verification

For a pair of intersected bounding boxes (Fig. 5b,c), the distances between the points of the powerline segment and the individual tree will be calculated in an ergodic way. If any of them is less than the required safe value, the tree encroachment will be deemed to occur (Fig. 5c). When the tree encroachment is detected, the encroaching tree and its coordinate position will be conveniently acquired. Then the powerline inspector should be sent to verify it on site, as there is a possibility of false detection of tree encroachment. If the tree encroachment is verified, the identified encroaching trees will be felled accordingly.

4. Experiments and results

4.1. Classified and segmented point cloud

As shown in Fig. 6, the point cloud of the powerline corridor was classified into ground, powerline, tower, and vegetation. The ground points was well separated from non-ground points using cloth filtering, even in the areas of steep terrain. Also, the powerline and the tower was well distinguished at the intersected parts using the DECF method. Thus, the points of the lowest powerline was further extracted. Although the vegetation was generally well extracted, some misclassifications occurred around the two towers. When the tower points were extracted, the vegetation points in the surrounding cylinder was falsely classified as the tower points. However, the misclassified vegetation points would not affect subsequent tree encroachment detection, as the vegetation nearby the towers was mostly low shrubs.

According to the tree density in the test site, the distance threshold was set as 2 m in the individual tree segmentation. A total of 155 individual trees were initially extracted from the vegetation points in the vicinity of the powerline corridor. Due to tree canopy occlusion and terrain influence, there existed some cases of insufficient segmentation or over- segmentation. According to visual judgment and field investigation, 134 individual trees were finally retained, and the segmentation accuracy was 86.54%. As shown from the side view in Fig. 7a, the resulting individual trees were rendered in various colors. Among them, there were 87 Masson pine and 47 Eucalyptus. They were sequentially numbered and separately circled according to the tree species as seen in the top view (Fig. 7b). At the same time, the current individual tree heights were extracted.

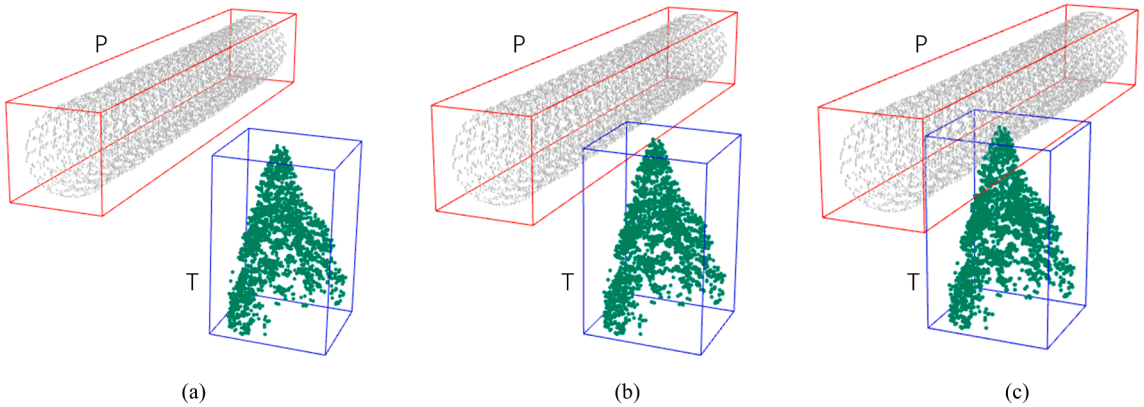

Fig. 5. Bounding box intersection test and tree encroachment detection. (a) P and T are not intersected; (b) P and T are intersected but tree encroachment does not occur; (c) P and T are intersected and tree encroachment occurs.

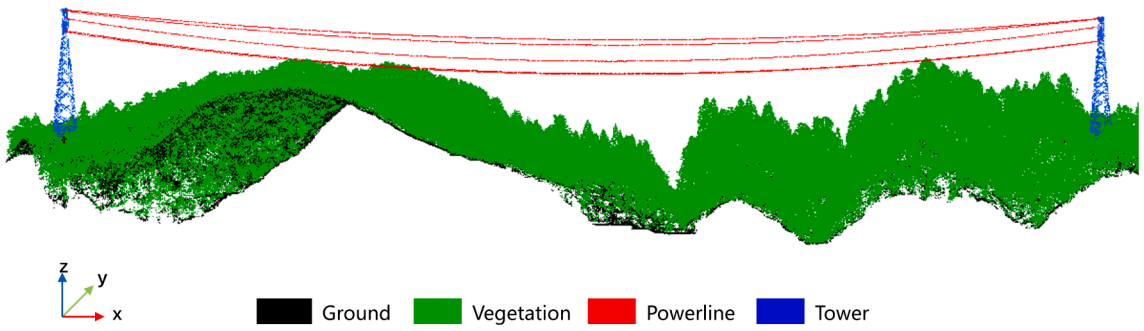

Fig. 6. Classified point cloud of the powerline corridor.

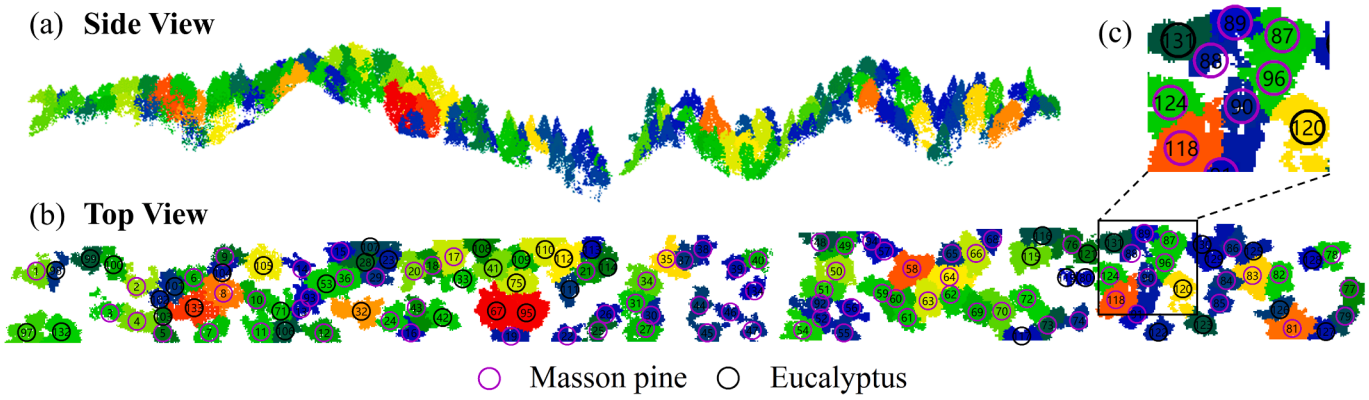

Fig. 7. Individual trees rendered in colors: (a) from the side view; (b) numbered and circled tree species from the top view; (c) one rectangular part of the top view was zoomed in.

4.2. Fitted tree growth models

With the tree plot statistical data, the Richards growth models of Masson pine and eucalyptus were separately fitted. The model parameters *a*, *b*, *c* of the two tree species were estimated as 21.221, 0.078, 1.212, and 26.547, 0.118, 1.345 respectively. According to the fitting curves shown in Fig. 8a, b, the growth processes of the two tree species were generally similar, showing the characteristics from initially rapid to slow in middle, and finally convergent to the maximum heights. The deflection points of the curves both appeared around the age of 20 yr. But for specific growth stages, the two tree species were somewhat different. First, the model parameter *a* showed that the maximum tree heights of Masson pine and eucalyptus were 21.221 m and 26.547 m, respectively. Secondly, the eucalyptus grew rapidly in the young ages, especially between 5 yr and 15 yr.

4.3. Pre-detected tree encroachment

With the two fitted Richards growth models, we acquired the individual tree heights in the powerline corridor in the next 10 years (year 0 represented the current year). Then, the Z coordinate values of the points belonging to the individual trees were added with the

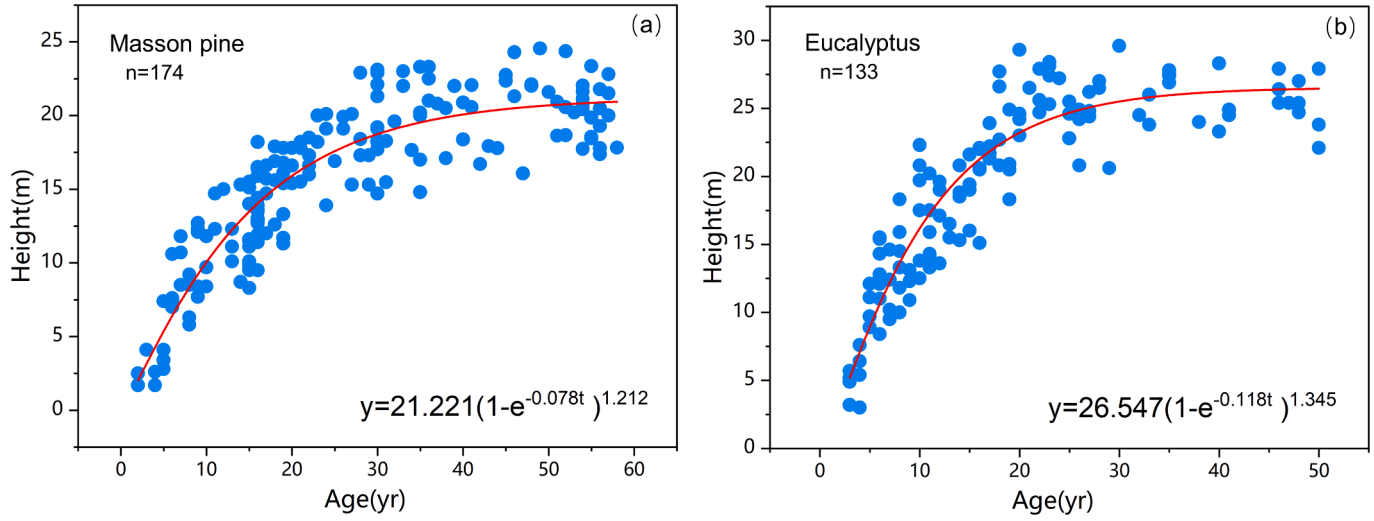

Fig. 8. The fitting curves of Richards growth models of Masson pine and Eucalyptus.

corresponding tree height increment. The bounding boxes of the individual trees were normally generated for the current year. For the subsequent years, the bounding boxes only needed to add the corresponding tree height increment in the Z axis. The 3D buffer with a radius of 6 m (the required safe distance) was generated for the powerline in the corridor. After repeated experiments, 50 m was found to be an appropriate unit length of segment to attain fair efficiency. Therefore, the powerline buffer was divided into 10 segments, and their bounding boxes were then produced. Lastly, the two-phase tree encroachment detection method was used to detect the unsafe points and identify the trees encroaching into the powerline corridor. The encroaching points in year 0, 1, 2, 5 and 10 were shown in Fig. 9a from the top view and Fig. 9b from the side view. Moreover, the corresponding encroaching individual trees were also identified, which were indicated in Fig. 10a from the top view and Fig. 10b from the side view.

According to Table 2 and year 0 in Fig. 9, there were tree encroachments occurring in current conditions, which were mainly distributed in the two regions with high elevations. Among them, the clearance distances between the powerline and trees ranged from 3.94 m to 5.67 m. In the following two years, although the detected unsafe points increased (Fig. 9), the detected encroaching trees did not change (Fig. 10). From year 3, there was basically one or more new encroaching trees every year. Therefore, it was necessary to model the tree growth and applied the results to early detection and warning of tree encroachment. As shown in Table 2, most of the new encroaching trees are Eucalyptus. This is because Eucalyptus is a fast-growing tree species, and the local subtropical climate is very suitable for its growth. Therefore, Eucalyptus should be taken as the key tree species while detecting tree encroachment in the powerline corridors of this region.

In practice, once the tree encroachment is pre-detected at the given time point, the powerline inspector should be sent to verify it on site when the time point comes into present. If the tree encroachment does occur, the identified encroaching trees will be felled. Thus, the underneath forest in the powerline corridor has been changed. Alternatively, all these pre-detected encroaching trees can be removed at one time to ensure the local safety of power transmission in the next 10 years. Whether potential encroaching trees are permitted to be felled and how long is the future time span will be determined by the policies coordinately formulated by local electric power sector and forestry authorities. Anyhow, the manual and financial cost of powerline inspection will be substantially reduced.

4.4. Accuracy assessment

It is generally difficult to assess the accuracy of tree encroachment detection at a given time point of years later. Actually, the final accuracy mostly depends on the accuracy of the extracted individual tree heights and the fitting degrees of Richards growth models.

4.4.1. Accuracy of extracted individual tree heights

From the extracted individual trees in the powerline corridor, 55 sample trees were selected to measure their real heights in the field. The composition of tree species and the spatial distribution of sample trees were also considered in the selection. Then the heights extracted from tree points were assessed against the measured ones. The coefficient of determination (R^2) and root mean square error (RMSE) were used as the criteria. As shown in Fig. 11, the R^2 was 0.923 and the RMSE was 1.107 m, which indicated that there was a high correlation between the extracted and measured tree heights. Therefore, the extracted individual tree heights could basically satisfy the requirements of predicting individual tree heights with Richards growth model.

4.4.2. Fitting degrees of Richards growth models

As mentioned in Section 2.2.2, the rest 20% plot data of the two tree

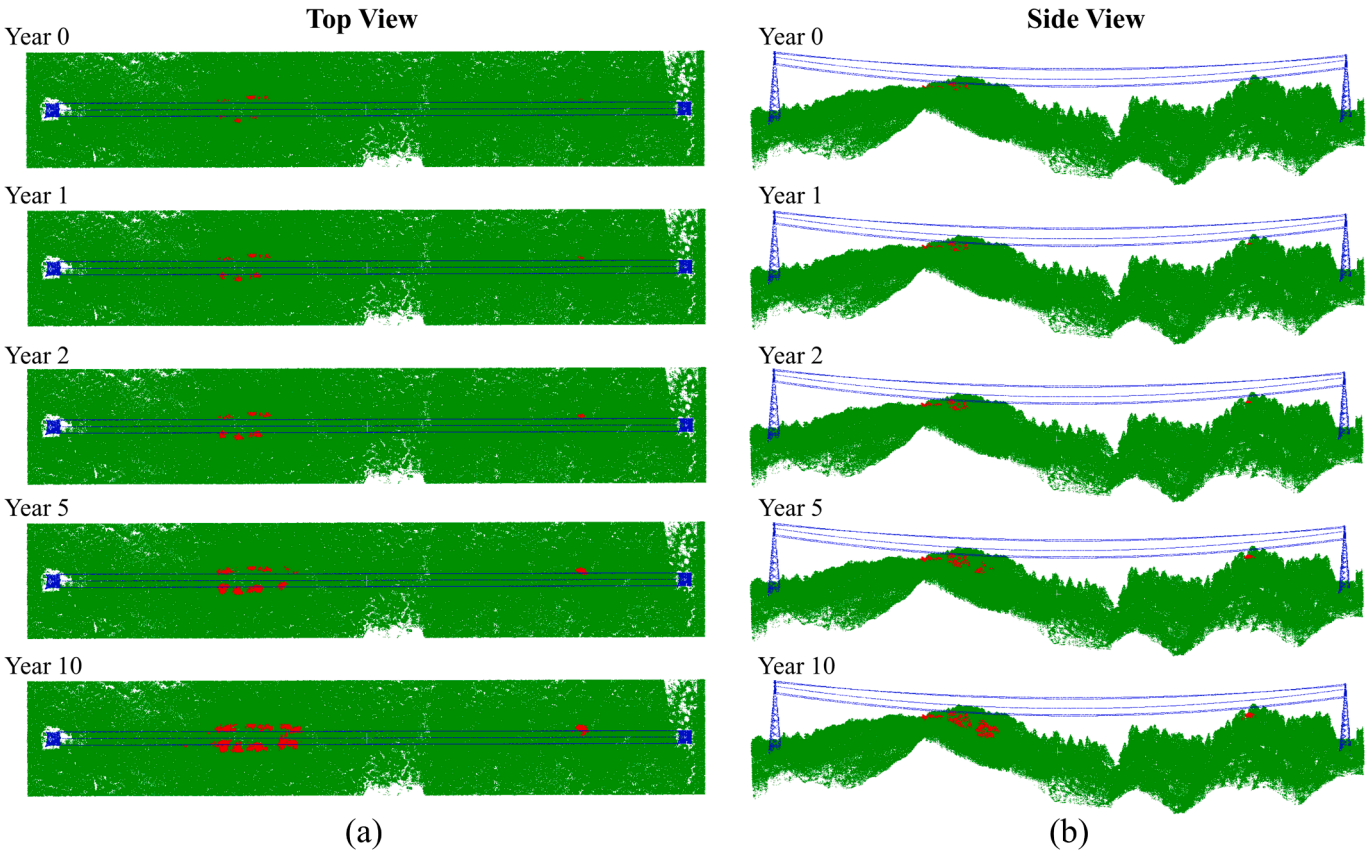

Fig. 9. Detected encroaching points in year 0, 1, 2, 5 and 10. (a) from the top view; (b) from the side view.

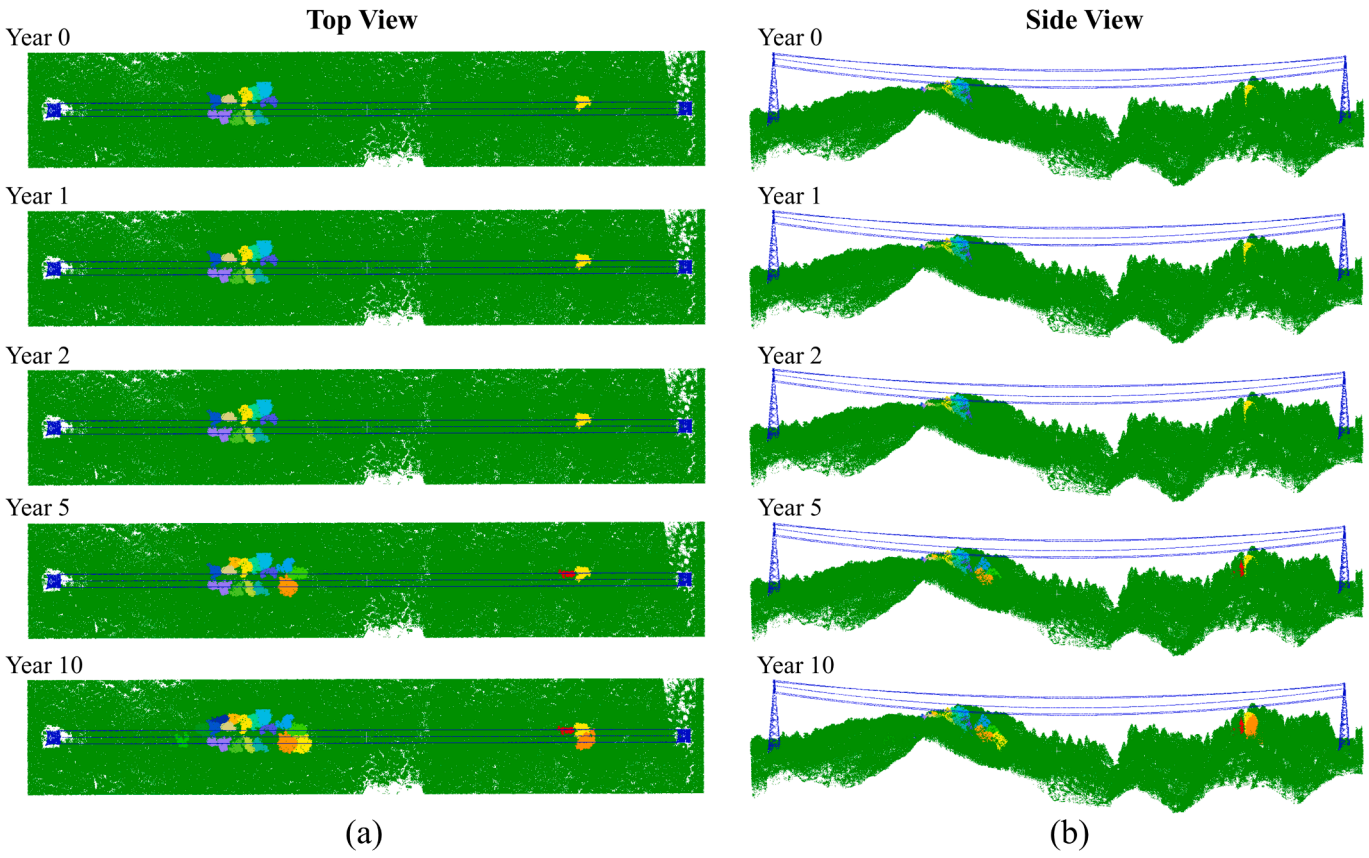

Fig. 10. Identified encroaching individual trees in year 0, 1, 2, 5 and 10. (a) from the top view; (b) from the side view.

Table 2
The data of pre-identified encroaching trees in the sample segment of the powerline corridor.

Tree No.	Tree species	Tree Coordinate (x, y)	Time point in future (yr)	Clearance distance (m)
17	Masson pine	516003.63,2958399.25	0	5.12
18	Masson pine	516004.97,2958392.75	0	4.12
20	Masson pine	516006.47,2958388.25	0	3.94
24	Masson pine	516024.84,2958372.75	0	4.62
29	Masson pine	516005.88,2958370.25	0	4.33
32	Eucalyptus	516017.38,2958362.51	0	4.58
33	Eucalyptus	516016.16,2958401.27	0	4.38
36	Masson pine	516004.51,2958365.12	0	5.22
42	Eucalyptus	516027.16,2958387.51	0	4.47
43	Masson pine	516027.53,2958382.75	0	5.67
124	Masson pine	516103.25,2958632.33	0	5.41
23	Eucalyptus	516032.06,2958410.25	3	4.67
41	Eucalyptus	516014.53,2958418.14	4	5.82
67	Eucalyptus	515998.97,,2958377.98	5	5.80
75	Eucalyptus	516025.84,2958420.58	5	5.08
80	Eucalyptus	516104.09,2958625.20	5	5.78
28	Eucalyptus	516000.38,2958372.75	6	5.87
53	Eucalyptus	516004.88,2958356.75	6	5.47
71	Eucalyptus	516008.19,2958336.53	8	5.27
95	Eucalyptus	516036.63,2958423.75	10	5.74
118	Masson pine	516111.53,2958633.58	10	5.92

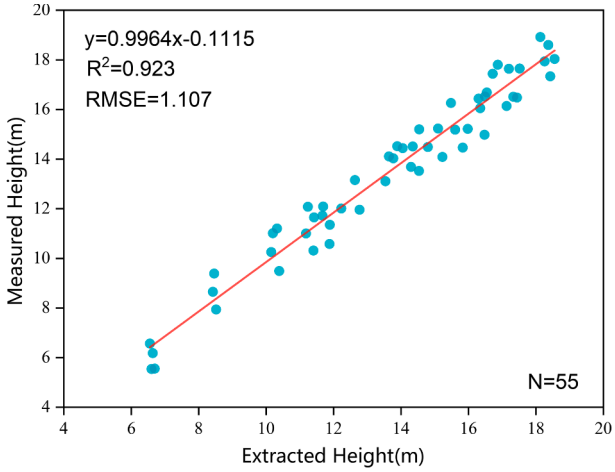

Fig. 11. Accuracy assessment of extracted individual tree heights from point cloud.

species were used to evaluate the fitting degrees of Richards growth models in Fig. 8. As shown in Fig. 12, the R^2 of Richards model of Masson pine and Eucalyptus were 0.812 and 0.861, and the RMSE were 2.308 m and 2.556 m, which were relatively small compared with the mean tree heights. Therefore, the two Richards growth models demonstrated good fitting degrees, and suitable for predicting the individual tree heights at the given time points in the future.

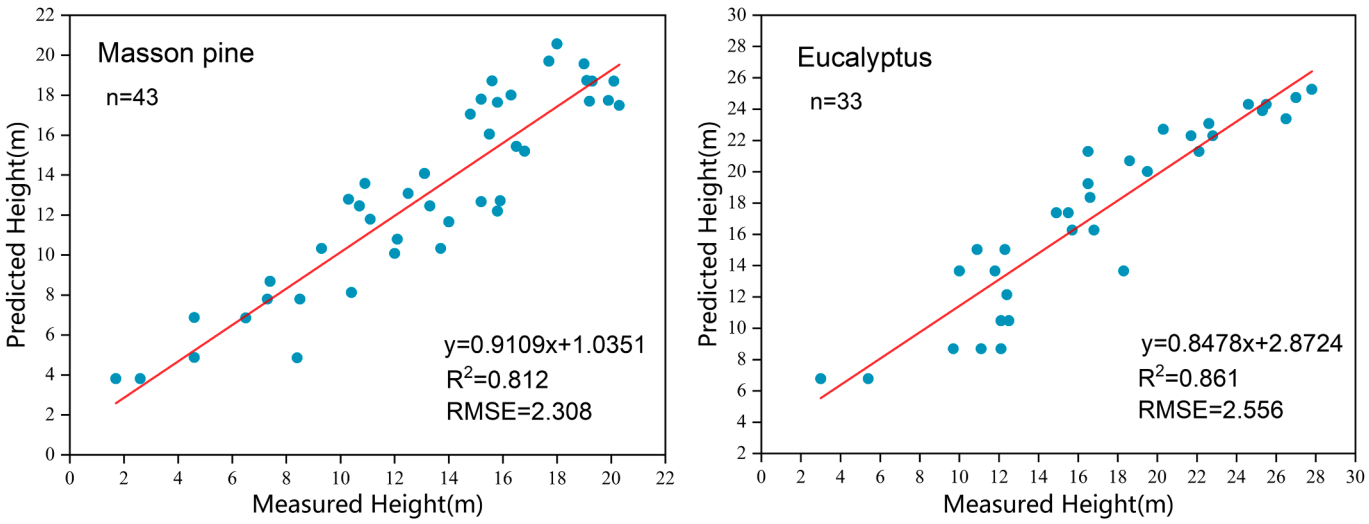

Fig. 12. Fitting degree evaluation of Richards growth models of Masson pine and Eucalyptus.

5. Discussion

5.1. Comparison of tree growth models

We chose the other four popular tree growth models including two theoretical models(Logistic and Gompertz) and two empirical models (Hyperbolic and Schumacher) to compare their adaptabilities in modelling tree growth with Richards model. Their model equations and parameters were listed in Table 3 (Fekedulegn et al., 1999; Abrantes et al., 2019). The parameters of the two theoretical models had the same biological significances as Richards model (see Section 3.2.1). But for the two empirical models, their parameters had no biological significance.

The five tree growth models were separately fitted with the 80% tree plot data of Masson pine and Eucalyptus. As shown in Fig. 13a, b, the five fitting curves of each tree species had a generally similar pattern at the three growth stages (young, middle, and old age). Normally, a complete growth curve should satisfy the two boundary constraints: $y(t) = 0$ when t approaches zero; $y(t) = A$ when t approaches infinity (A is a constant value, namely the maximum possible tree height of a tree species). According to the starting ends of the five fitting curves, the Richards, Hyperbolic and Schumacher models exhibited a natural tendency to be 0 m when the tree age approached zero, but the Logistic and Gompertz models did not. As for the terminal ends of those fitting curves, the Richards, Logistic and Gompertz models indicated a tendency to converge to a constant height, but Hyperbolic and Schumacher models did not. Only Richards model fairly satisfied the aforementioned two constraint conditions. In addition, as listed in Fig. 13a, b, Richards model had the highest R^2 (0.831 and 0.855) and the lowest RMSE (2.189 m and 2.876 m) among the five growth models for Masson pine and eucalyptus, respectively. Therefore, Richards growth model demonstrated the optimum adaptability for modelling tree growth in the study area among the five growth models.

Table 3
The equations and parameters of the other four tree growth models.

Model name	Model equation	Model type	Model parameters
Logistic	$y = a/(1 + be^{-ct})$	Theoretical	a, b, and c have the same biological significances as Richards model.
Gompertz	$y = ae^{-be^{-ct}}$	Theoretical	a, b, and c have the same biological significances as Richards model.
Hyperbolic	$y = a - b/(t+c)$	Empirical	a, b, and c have no biological significances.
Schumacher	$y = ae^{-b/t}$	Empirical	a and b have no biological significances.

t is the tree age and y represents the tree height at t age.

5.2. Comparison of algorithm performances

In the study, the point traversal algorithm and two-phase algorithm for tree encroachment detection were implemented using C++ programming language and point cloud library (PCL). We first compared their processing time consumptions at the time points of year 0, 1, 2, 5, and 7. As shown in Fig. 14a, the average time consumptions of point traversal algorithm and two-phase algorithm were about 760 s and 10 s, respectively. The former was nearly 76 times of the latter. Moreover, the time consumption of two-phase algorithm decreased from year 1 to 7. That was because it spent more time on bounding box generation for individual trees in year 0(Fig. 14b). Thereafter, the new bounding boxes for individual trees were simply generated by adding the increment of predicted tree heights to the original ones in the Z axis.

To further compare the performances of the two algorithms with the increase of point number, the other 4 segments of the Chixin powerlines were selected and numbered from 2 to 5. Likely, the dominant tree species in their underneath forest were Masson pine and Eucalyptus. As shown in Fig. 15a, their processing time consumptions generally increased with the increment of point number. Furthermore, the former increased significantly more than the latter. However, the Segment 4, 5 were seemingly not in line with this trend. It was because the point numbers listed in Fig. 15a were actually the tree points in those segments. But the total time consumption was jointly decided by both tree points and powerline points. As seen in Fig. 15b, the point number of powerlines in Segment 4, 5 had a marked increase. Additionally, the processing time of two-phase algorithm largely depended on the number of initial and intersected bounding boxes. In sum, the two-phase algorithm further outperformed point traversal algorithm with the increase of point number.

5.3. Error sources and potential improvements

Although the proposed method of early detecting tree encroachment in powerline corridor using growth model and UAV-borne LiDAR was effective and efficient, there were still some factors that probably affected its applications. For instance, the tree species of segmented individual trees were determined by combining visual interpretation and field investigation, and it was not applicable for long-distance powerline corridors. Although the accuracy of extracted individual tree height was relatively high, some errors were unavoidably

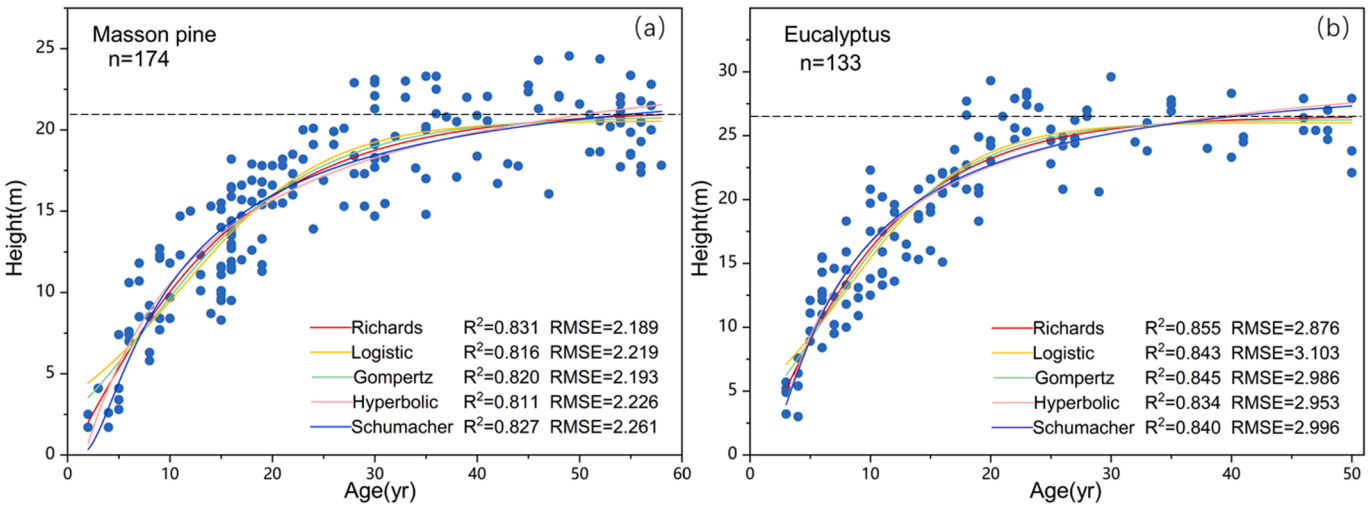

Fig.13. Fitting curves of the five growth models of Masson pine and Eucalyptus.

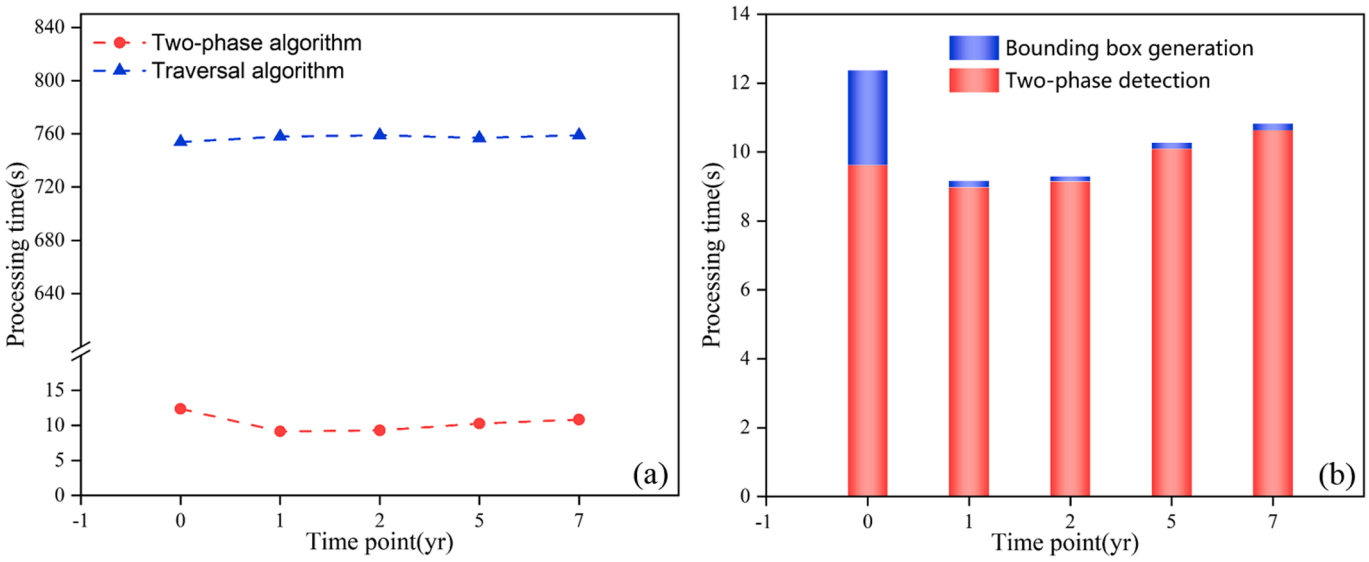

Fig. 14. Processing time consumptions in serial time points. (a) traversal algorithm and two-phase algorithm; (b) bounding box generation and two-phase detection.

transferred to the predicted individual tree heights at given time points. Additionally, the Richards growth models were fitted with the tree plot data of Masson pine and Eucalyptus, but the site conditions of the tree plots were not completely consistent with those of the individual trees in the powerline corridor. Therefore, some uncertainties were inevitably induced into the individual tree heights predicted by the Richards growth models. In this study, it was assumed that the 3D position of the powerlines was fixed and stable. However, in reality the status of the powerlines would slightly oscillate with changes of environmental conditions such as the temperature and the wind (Zhang et al., 2020b).

Nevertheless, some measures could be taken to further improve the early detection of tree encroachment. For example, point cloud data can be used to extract structural parameters and morphological features of individual trees, and the tree species can be automatically recognized using the corresponding classifiers (Chen et al., 2019). Furthermore, there have been many studies on the application of machine learning or deep learning to intelligent tree species classification (Kattenborn et al., 2021). In addition, the hierarchical bounding boxes can be generated to enclose the individual tree structure, so as to further reduce the time complexity of intersection test and improve efficiency (Yu et al., 2018). Lastly, the status variation of powerlines in various environmental conditions can be modeled (Jaw and Sohn, 2017), and integrated into our method in the future research. Anyway, it is very important to verify the early detected tree encroachment on site, and make corresponding treatments.

6. Conclusions

In this study, we attempted to apply UAV-borne LiDAR and tree growth model to early detecting tree encroachment in high voltage powerline corridor. The major conclusions we reached are as follows:

- UAV-borne LiDAR is a powerful technique to acquire point cloud data of the powerline corridor, from which the individual trees and their heights can be accurately extracted. The R^2 of the extracted individual tree heights was 0.923 and the RMSE was 1.107 m.
- Among the five theoretical and empirical tree growth models, Richards model demonstrated the optimum adaptability for modelling tree growth. Only Richards model simultaneously satisfied the two constraint conditions, and its fitting curve had the highest R^2 (0.831 and 0.855) and the lowest RMSE (2.189 m and 2.876 m) for Masson pine and eucalyptus, respectively.

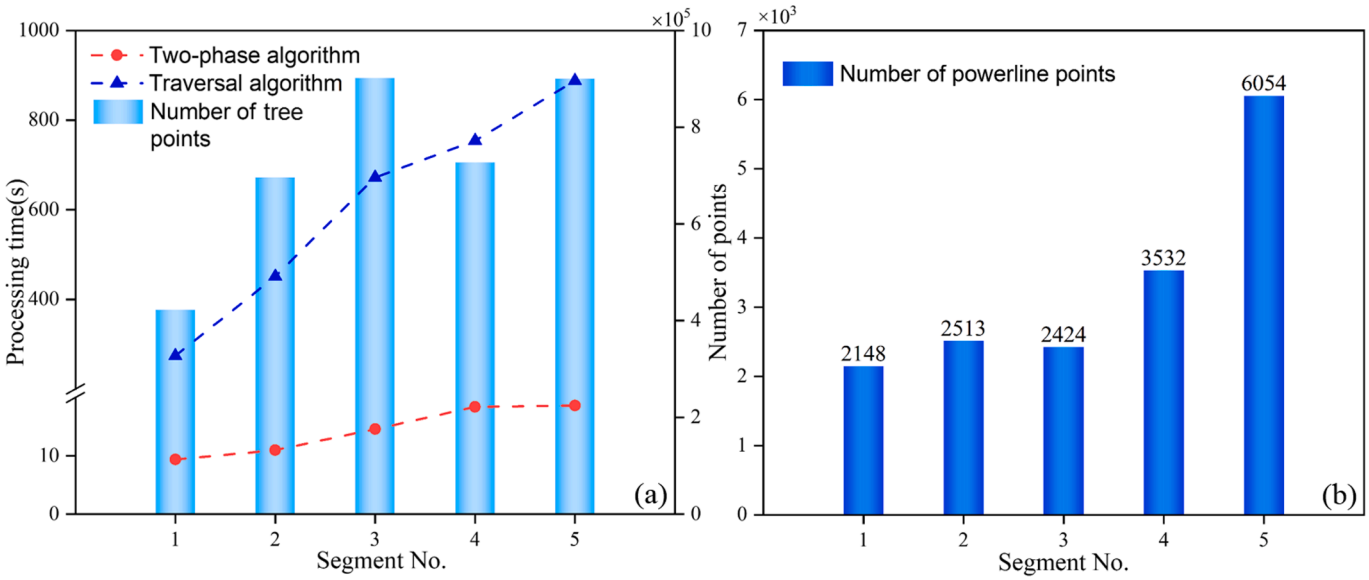

Fig. 15. Processing time consumptions in serial segments of the powerline corridor. (a) traversal algorithm and two-phase algorithm; (b) numbers of powerline points.

- Compared with point traversal algorithm, the calculation efficiency of the bounding box-based two-phase algorithm for tree encroachment detection was improved by nearly 76 times on average. 50 m was found to be an appropriate unit length for segmenting 3D powerline buffer through repeated experiments.
- Once potential tree encroachments are pre-detected in powerline corridors at a future time point, the powerline inspectors can be sent out to verify and fell encroaching trees when the time point comes into present. The powerline inspection becomes targeted, avoiding periodically inspecting the whole corridors, thus the inspection efficiency will be greatly improved.

Although our study provides the effective method to early detect tree encroachment in powerline corridors using a UAV-borne LiDAR, there were some factors that affected its applications including non-automated tree species recognition, errors in individual tree height extraction and prediction, and unstable positions of powerlines, and so forth. Therefore, it is still a very challenging task to accurately detect tree encroachment in powerline corridors at the early stage. In practice, we have to confirm the pre-detected tree encroachments on site and make proper treatments. In future studies, the intelligent recognition of underneath tree species should be taken into consideration and the statuses of powerlines varying with environmental conditions should be modeled.

CRediT authorship contribution statement

Yangyu Chen: Methodology, Formal analysis, Data curation, Writing – original draft. **Jiayuan Lin:** Conceptualization, Methodology, Formal analysis, Investigation, Writing – review & editing. **Xiaohan Liao:** Funding acquisition, Investigation.

Declaration of Competing Interest

The authors declare that they have no known competing financial interests or personal relationships that could have appeared to influence the work reported in this paper.

Acknowledgements

This paper was jointly supported by the Strategic Priority Research Program of the Chinese Academy of Sciences (grant no. XDA19050501), the National Natural Science Foundation of China (grant no. 32071678), and the Key Research and Development Program of the Sichuan Province (grant no. 22QYCX0156). The authors would like to thank Li Zhang from Fengmai Intelligent Technology (Chongqing) Co., Ltd, Shaopan Zeng and Zhenlu Liao from Sanming Power Supply Company of State Grid Fujian Electric Power Co., Ltd, China for their help in acquiring LiDAR point cloud of the powerline corridor in the test site and providing local tree plot data of Masson pine and Eucalyptus.

References

Abrantes, K.K.B., Paiva, L.M., de Almeida, R.G., Urbano, E., Ferreira, A.D., Mazucheli, J., 2019. Modeling the individual height and volume of two integrated crop-livestock-forest systems of Eucalyptus spp. in the Brazilian Savannah. Acta Sci.-Agron. 41, 8. https://doi.org/10.4025/actasciagron.v41i1.42626.

Ahmad, J., Malik, A.S., Xia, L., Ashikin, N., 2013. Vegetation encroachment monitoring for transmission lines right-of-ways: A survey. Electr. Power Syst. Res. 95, 339–352. https://doi.org/10.1016/j.epsr.2012.07.015.

ASPRS, 2005. LAS 1.4 specification approved by ASPRS board. Retrieved August 22nd, 2021 from https://www.asprs.org/divisions-committees/lidar-division/laser-las-file-format-exchange-activities.

Azevedo, F., Dias, A., Almeida, J., Oliveira, A., Ferreira, A., Santos, T., Martins, A., Silva, E., 2019. LiDAR-based real-time detection and modeling of power lines for Unmanned Aerial Vehicles. Sensors 19 (8), 1812–1839. https://doi.org/10.3390/s19081812.

Calama, R., Barbeito, I., Pardos, M., del Rio, M., Montero, G., 2008. Adapting a model for even-aged Pinus pinea L. stands to complex multi-aged structures. For. Ecol. Manage. 256 (6), 1390–1399. https://doi.org/10.1016/j.foreco.2008.06.050.

Chen, C., Yang, B., Song, S., Peng, X., Huang, R., 2018. Automatic clearance anomaly detection for transmission line corridors utilizing UAV-borne LiDAR data. Remote Sens. 10 (4), 613–633. https://doi.org/10.3390/rs10040613.

Chen, X., Yun, T., Xue, L., Liu, Y.a., 2019. Classification of tree species based on LiDAR point cloud data. Laser. Optoelectron. prog., 56(12), 203-214. 10.3788/LOP56.122801. (in Chinese with English abstract).

Cheng, L., Tong, L., Wang, Y., Li, M., 2014. Extraction of urban power lines from vehicle-borne LiDAR data. Remote Sens. 6 (4), 3302–3320. https://doi.org/10.3390/rs6043302.

Collet, C., Chenost, C., 2006. Using competition and light estimates to predict diameter and height growth of naturally regenerated beech seedlings growing under changing canopy conditions. Forestry 79 (5), 489–502. https://doi.org/10.1093/forestry/cpl033.

Dihkan, M., Mus, E., 2021. Automatic detection of power transmission lines and risky object locations using UAV LiDAR data. Arab. J. Geosci. 14 (7) https://doi.org/10.1007/s12517-021-06947-1.

Ding, W., Huang, X., Tan, X., Peng, J., Yu, H., Nie, D., 2018. Detecting danger vegetation in powerline corridors using airborne laser points. Geomat. Inf. Technol. 41 (11), 125–128. https://doi.org/10.3969/j.issn.1672-5867.2018.11.036 in Chinese with English abstract.

Fan, J., 2012. The modified Levenberg-Marquardt method for nonlinear equations with cubic convergence. Math. Comput. 81, 447–466.
Fekedulegn, D., Mac Siurtain, M.P., Colbert, J.J., 1999. Parameter estimation of nonlinear growth models in forestry. Silva Fennica. 33 (4), 327–336. https://doi.org/10.14214/sf.653.
Fox, J.C., Ades, P.K., Bi, H., 2001. Stochastic structure and individual-tree growth models. For. Ecol. Manage. 154 (1–2), 261–276. https://doi.org/10.1016/S0378-1127(00)00632-0.
Fu, H.A., Wang, X., Tian, S., Ma, H., Xia, J., 2019. Corridor cleaning method for power transmission line based on UAV LiDAR technique. Electr Meas. Instrum. 56 (23), 146–152. https://doi.org/10.19753/j.issn1001-1390.2019.023.022 in Chinese with English abstract.
Gottschalk, S., Lin, M.C., Manocha, D., 1996. OBB tree: a hierarchical structure for rapid interference detection. In: proceedings of the 23rd annual conference on computer graphics and interactive techniques, 171-180. 10.1145/237170.237244.
Guan, H., Yu, Y., Li, J., Ji, Z., Zhang, Q., 2016. Extraction of power-transmission lines from vehicle-borne Lidar data. Int. J. Remote Sens. 37 (1), 229–247. https://doi.org/10.1080/01431161.2015.1125549.
Guo, B., Li, Q., Huang, X., Wang, C., 2016. An improved method for power-line reconstruction from point cloud data. Remote Sens. 8 (1), 36–52.
Hartling, S., Sagan, V., Maimaitijiang, M., Dannevik, W., Pasken, R., 2021. Estimating tree-related power outages for regional utility network using airborne LiDAR data and spatial statistics. Int. J. Appl. Earth Obs. Geoinf. 100, 15. https://doi.org/10.1016/j.jag.2021.102330.
Huang, W., Huang, Z., Wang, L., Jiang, S., Feng, B., 2017. Dynamic management and early-warning analysis of tree barrier hidden danger in overhead transmission line corridor. Guangxi Electric Power 40 (03), 39–42. https://doi.org/10.16427/j.cnki.issn1671-8380.2017.03.011 in Chinese with English abstract.
Huang, W., Jiang, S., He, S., Jiang, W.S., 2021. Accelerated multi-view stereo for 3D reconstruction of transmission corridor with fine-scale power line. Remote Sens. 13 (20), 4097.
Jaw, Y., Sohn, G., 2017. Wind adaptive modeling of transmission lines using minimum description length. ISPRS J. Photogramm. Remote Sens. 125, 193–206. https://doi.org/10.1016/j.isprsjprs.2017.01.013.
Kattenborn, T., Leitloff, J., Schiefer, F., Hinz, S., 2021. Review on Convolutional Neural Networks (CNN) in vegetation remote sensing. ISPRS J. Photogramm. Remote Sens. 173, 24–49. https://doi.org/10.1016/j.isprsjprs.2020.12.010.
Li, P., Wu, H.E., Jing, J., Li, R., 2016. Noise classification denoising algorithm for point cloud model. Comput. Eng. Appl. 52 (20), 188–192. https://doi.org/10.3778/j.issn.1002-8331.1603-0354 in Chinese with English abstract.
Li, W., Guo, Q., Jakubowski, M.K., Kelly, M., 2012. A new method for segmenting individual trees from the Lidar point cloud. Photogramm. Eng. Remote Sens. 78 (1), 75–84. https://doi.org/10.14358/PERS.78.1.75.
Lin, J.Y., Shu, L., Zuo, H., Zhang, B.S., 2012. Experimental observation and assessment of ice conditions with a fixed-wing unmanned aerial vehicle over yellow river. China. J. Appl. Remote Sens. 6 (1), 3586–3597.
Liu, H., Cheng, Y., Liu, B., 2019. Analysis of potential tree damage and vegetation management strategy in transmission corridor. Heilongjiang Electr Power 41 (1), 64–67. https://doi.org/10.13625/j.cnki.hljep.2019.01.013 in Chinese with English abstract.
Ma, J., Cheng, J.C.P., Jiang, F.F., Gan, V.J.L., Wang, M.Z., Zhai, C., 2020. Real-time detection of wildfire risk caused by powerline vegetation faults using advanced machine learning techniques. Adv. Eng. Inform. 44, 101070–101078. https://doi.org/10.1016/j.aei.2020.101070.
Matikainen, L., Lehtomaki, M., Ahokas, E., Hyyppa, J., Karjalainen, M., Jaakkola, A., Kukko, A., Heinonen, T., 2016. Remote sensing methods for power line corridor surveys. ISPRS J. Photogramm. Remote Sens. 119, 10–31. https://doi.org/10.1016/j.isprsjprs.2016.04.011.
Mills, S.J., Castro, M.P.G., Li, Z., Cai, J., Hayward, R., Mejias, L., Walker, R.A., 2010. Evaluation of aerial remote sensing techniques for vegetation management in power-Line corridors. IEEE Trans. Geosci. Remote Sens. 48 (9), 3379–3390. https://doi.org/10.1109/TGRS.2010.2046905.
Nguyen, V.N., Jenssen, R., Roverso, D., 2018. Automatic autonomous vision-based power line inspection: a review of current status and the potential role of deep learning. Int. J. Electr. Power Energy Syst. 99, 107–120. https://doi.org/10.1016/j.ijepes.2017.12.016.
Ortega, S., Trujillo, A., Santana, J.M., Suarez, J.P., Santana, J., 2019. Characterization and modeling of power line corridor elements from LiDAR point clouds. ISPRS J. Photogramm. Remote Sens. 152, 24–33. https://doi.org/10.1016/j.isprsjprs.2019.03.021.
Palmer, I.J., Grimsdale, R.L., 1995. Collision detection for animation using sphere-trees. Comput. Graph. Forum. 14 (2), 105–116. https://doi.org/10.1111/1467-8659.1420105.
Ruan, J., Tao, X., Wei, X., LIi, H., 2019. 3D modeling and tree barrier analysis of transmission lines based on LiDAR point cloud data of fixed wing UAV. South. Energy. Constr. 6 (1), 114–118. https://doi.org/10.16516/j.gedi.issn2095-8676.2019.01.020 in Chinese with English abstract.
Shi, Z., Lin, Y., Li, H., 2020. Extraction of urban power lines and potential hazard analysis from mobile laser scanning point clouds. Int. J. Remote Sens. 41 (9), 3411–3428. https://doi.org/10.1080/01431161.2019.1701726.
Shoda, T., Imanishi, J., Shibata, S., 2020. Growth characteristics and growth equations of the diameter at breast height using tree ring measurements of street trees in Kyoto City, Japan. Urban For. Urban Green. 49, 126627 https://doi.org/10.1016/j.ufug.2020.126627.
Tang, L., Song, W.G., Hou, T.C., Liu, L.L., Cao, W.X., Zhu, Y., 2018. Collision detection of virtual plant based on bounding volume hierarchy: a case study on virtual wheat. J. Integr. Agric. 17 (2), 306–314. https://doi.org/10.1016/S2095-3119(17)61769-6.
Wang, Y.J., Chen, Q., Liu, L., Zheng, D.Y., Li, C.K., Li, K., 2017. Supervised Classification of Power Lines from Airborne LiDAR Data in Urban Areas. Remote Sens. 9 (8), 771–786.
Wei, X., Sun, Y., Ma, W., 2012. A height growth model for Cunninghamia lanceolata based on Richards'equation. J. Zhejiang Agric. For. Univ. 29 (5), 661–666. https://doi.org/10.11833/j.issn.2095-0756.2012.05.004 in Chinese with English abstract.
Wu, J.Q., Liu, H., Yang, J., Chen, Y., 2021. Tree barrier prediction of power lines based on tree height growth model. IOP Conf. Ser.: Earth Environ. Sci. 645 (1) https://doi.org/10.1088/1755-1315/645/1/012008.
Xing, Y.S., Liu, X.P., Xu, S.P., 2010. Efficient collision detection based on AABB trees and sort algorithm. In: IEEE 2010 8th International Conference on Control and Automation, 328-332. 10.1109/icca.2010.5524093.
Yu, R., Zhao, J., Yu, L., Zhang, Q., 2018. Collision detection algorithm based on AABB bounding box and space division. J. Image Graph. 23 (12), 1925–1937. https://doi.org/10.11834/jig.180050 in Chinese with English abstract.
Zhang, S., Qi, L.Z., Han, W.J., 2020a. Danger tree detection and tree number estimation based on UAV LiDAR data. J. Univ. Chin. Acad. Sci. 37 (6), 760–766. https://doi.org/10.7523/j.issn.2095-6134.2020.06.006 in Chinese with English abstract.
Zhang, S.C., Liu, J.Z., Niu, Z., Gao, S., Xu, H.Z., Pei, J., 2020b. Power line simulation for safety distance detection using point clouds. IEEE Access. 8, 165409–165418. https://doi.org/10.1109/ACCESS.2020.3022670.
Zhang, W., Qi, J., Wan, P., Wang, H., Xie, D., Wang, X., Yan, G., 2016. An easy-to-use airborne LiDAR data filtering method based on cloth simulation. Remote Sens. 8 (6), 501–522. https://doi.org/10.3390/rs8060501.